# Heuristic Approach to Indoor Localization Using LoRa RSSI Measurements

*Reynel OLIVERA [1,3], Jorge FLORES [2], Roberto OLIVERA [1,3], Janette PEREZ [3], Jorge MUNOZ [1]*

[1] Electrical Engineering, Autonomous University of Zacatecas, Fraccionamiento Solidaridad, Jalpa, 99601, Zacatecas, México
[2] Electrical Engineering, Autonomous University of Zacatecas, 801 Ramon Lopez Velarde, Zacatecas 98000, Zacatecas, Mexico
[3] Graduate Program in Engineering for Technological Innovation, Electrical Engineering, Autonomous University of Zacatecas, Ramón López Velarde 801, Zacatecas 98000, Zacatecas, México

{reynel, jflorest, roliverar, r.perez, j.munoz}@uaz.edu.mx

Submitted April 8, 2025 / Accepted June 17, 2025 / Online first August 4, 2025

**Abstract.** *This research presents a heuristic approach for indoor localization using standard LoRa modules operating at 915 MHz. To overcome the challenges presented by signal attenuation, multipath propagation, and environmental variability, the proposed method combines Received Signal Strength Indicator (RSSI) based distance estimation with a path loss exponent tuned empirically for different environments. A trilateration algorithm based on Ordinary Least Squares (OLS) is employed to estimate target positions, and performance is enhanced using filtering techniques such as Median Filter (MF) and Moving Average Filter (MAF). Additionally, two receiver geometries were analyzed to assess the robustness of the proposed method under different geometric configurations. To complement the OLS estimator, a Weighted Least Squares (WLS) method was also implemented using a Gauss–Newton optimization approach. While WLS shows promising results, further refinement of the covariance matrix $\boldsymbol{Q}$ is identified as a direction for future work. These findings underscore the potential of the approach as a low-cost, scalable solution for precise indoor localization in complex environments. Experimental evaluations conducted in various laboratory environments demonstrated that the optimized parameters yield a substantial reduction in positioning error. Performance was quantified using Mean Square Error (MSE), Root Mean Square Error (RMSE), and Mean Absolute Error (MAE) metrics, with MSE values as low as 0.2491 m in unfiltered scenarios, and as low as 0.07 m when applying MF and MAF with an appropriate window size. A brief analysis of results shows that an MF and MAF with window size $W_n = 7$ provides consistently adequate accuracy while keeping computational costs low.*

## Keywords

Indoor location, LoRa, heuristic approach, median filter

## 1. Introduction

Localization of objects in diverse environments, especially in healthcare, has been extensively studied and continues to grow in importance. Although this issue has been addressed using different technologies, selecting the ideal one remains challenging due to the diversity of physical variables. Energy consumption, communication distance, encryption and data storage, and environmental conditions are key factors to consider when choosing a particular technology [1]. Some proposed technologies, such as Wireless Fidelity (WiFi), Bluetooth Low Energy (BLE), Radio Frequency Identification (RFID), and, more recently, Long Range (LoRa), are the most well-known for localizing or tracking objects [2–4].

Although, LoRa is not commonly applicable for indoor location, several works have been developed to incorporate this technology in enclosed environments [5]. This task is complicated due to diffraction, refraction, and reflection of the transmitted signal, which are inherent to the natural propagation phenomena [6–8]. In addition to this, the number of objects can hinder the signal propagation and increase location errors [9–11].

In spite of the disadvantages of artifacts in the transmitted signal, the LoRa technology offers several strengths. Summarizing, LoRa offers long-range, low-power, scalable, and cost-effective communication. These advantages make LoRa especially suited for large IoT networks, remote monitoring, and environments where range and battery life are critical [12–14]. While Bluetooth, WiFi, and RFID are better for specific, short-range, high-bandwidth, or localized use cases, LoRa excels in long-range, low-power, and wide-area applications [15], [16].

The key to outperforming other technologies lies in the fact that LoRa communication encodes data based on the Chirp Spread Spectrum (CSS), where the frequency of the

DOI: 10.13164/re.2025.0509

signal continuously changes. The CSS technique allows the signal to spread over time, making it more resilient to noise and interference [17], [18]. The ability to adjust the spreading factor allows for a balance between range and data rate. LoRa is thus able to achieve long-range, low-power communication in different environments by utilizing chirp frequency shifts to encode information efficiently.

Determining the path loss exponent in indoor environments presents several challenges due to the complex and diverse nature of these spaces. The materials used in walls, ceilings, and furniture such as glass, wood, metal, and concrete affect signal propagation differently [2, 19, 20]. For instance, thicker walls or those made of denser materials like concrete can significantly attenuate signals, while glass or open partitions may have a lesser impact [21], [22]. Additionally, indoor environments are dynamic, with people moving and furniture being rearranged, introducing time dependent variations in path loss. Multipath propagation further complicates matters, as signals reflecting off surfaces can cause constructive or destructive interference [23]. These phenomena make it difficult to accurately measure the path loss exponent and necessitate careful calibration.

Another major challenge is obtaining accurate Received Signal Strength Indicator (RSSI) measurements. Hardware variability, noise, and environmental factors can affect these readings, making it difficult to derive consistent values for the path loss exponent. Selecting an appropriate reference distance and calibrating the reference path loss is critical, as it forms the baseline for estimating signal attenuation. Furthermore, shadowing effects caused by large or dense obstacles introduce randomness, typically modeled as a Gaussian variable, which further complicates the estimation process. To address these challenges, various approaches have been proposed. Site-specific calibration, involving detailed measurements in the target environment, is often used to tune the path loss exponent and other parameters.

In this work, we propose a heuristic approach for a fast estimation of the path loss exponent to different environments. Our methodology leverages real time RSSI measurements from standard 915 MHz LoRa modules and applies a trilateration algorithm based on Ordinary Least Squares enhanced by a median and a moving average filters to suppress measurement noise. To further boost accuracy, we also implement a weighted least squares estimator via a Gauss–Newton optimization, where the weighting matrix is derived from an empirically tuned covariance model $Q$. Two distinct receiver geometries, one compact and one widespread, are evaluated to assess robustness under varying spatial configurations. By calibrating the path loss exponent over a range of values and optimizing for minimal mean square error between predicted and actual positions, the approach adapts dynamically to various indoor conditions, thereby enhancing localization accuracy and reliability. For experimental tests, we selected a single LoRa signal configuration with a fixed Spreading Factor (SF) and Bandwidth (BW) to establish a consistent baseline for evaluating the proposed localization method. This choice simplifies the analysis by controlling signal characteristics, enabling focused optimization of the path loss exponent and filtering parameters. However, it is widely recognized that varying SF and BW settings affect signal range, sensitivity, and noise resilience, which may influence the accuracy of RSSI-based distance estimates. It is worth mentioning that experimental conditions were only partially controlled, as measurements were conducted in indoor classrooms without regulating the presence or movement of students and instructors to assess the robustness of the system to human interference. This intentional choice reflects realistic usage scenarios. However, a more exhaustive analysis of the structural of the building characteristics and installed equipment is required to fully understand their impact on localization performance.

## 1.1 Related Works

Recent studies have explored various approaches to RSSI-based localization using LoRa technology in indoor environments. For example, researchers have developed experiments to evaluate the accuracy of RSSI-based indoor localization, demonstrating significant reductions in localization error by optimizing the calibration of path loss models and leveraging advanced data processing techniques [2, 24–27]. These efforts underscore the potential of LoRa modules for applications in environments such as laboratories, hospitals, and smart homes, where precision is critical despite challenges like multipath propagation and Non-Line-of-Sight (NLOS) conditions [28–30]. However, these works propose different combinations of measurements [28], modifications to traditional algorithms [29], or the design of new devices and mechanisms to extract additional data [30].

Machine Learning (ML) algorithms are increasingly utilized in RSSI-based localization to improve accuracy by addressing NLOS propagation and environmental variability. For instance, Neural Networks (NNs) and Support Vector Machines (SVMs) have been applied to RSSI data for fingerprinting and path loss modeling, demonstrating significant improvements in localization precision compared to traditional deterministic methods [31–33]. However, these ML-based strategies have notable disadvantages. They often require large datasets for training, which may not be feasible in environments with limited measurements, such as laboratories. Moreover, their performance can be computationally intensive, making real-time localization challenging in resource-constrained devices. The generalization of ML models to different environments is another concern, as models trained in one setting may not perform well in others without extensive recalibration.

Our approach can be contrasted with recent RF based occupancy systems. For example, in [34] uses Wi-Fi probe requests as an RF fingerprint of the environment, they record raw Wi-Fi signals and input them into deep neural networks to detect occupancy and count people. Notably, their solution relies on available Wi-Fi infrastructure and extensive training

with real measurements. In contrast, our proposed method is based on 915 MHz LoRa RSSI measurements and a simple path loss model for trilateration. The method only requires calibration of the path loss exponent and the application of OLS or Weighted Least Squares (WLS) via Gauss–Newton (GN), combined with either a Median Filter (MF) or a Moving Average Filter (MAF), to estimate the target location. This avoids the need to build a full fingerprint database, instead, the system adapts to a new setting by quickly adjusting a small number of parameters.

The choice of 915 MHz LoRa (ISM band) was made for several reasons. First, 915 MHz lies in the unlicensed ISM band (902–928 MHz in Region 2), so no spectrum license is required [35], [36]. This simplifies the deployment of many devices across our laboratory environments. Second, the low frequency of LoRa enables long-range communication and effective building penetration. As a result, 915 MHz signals travel significantly farther and pass through walls more effectively than 2.4 GHz Wi-Fi signals [37]. Third, LoRa devices are low power and inexpensive, making large-scale deployment feasible [38]. Finally, although the low bandwidth of LoRa limits positioning accuracy to a few meters, its energy and cost efficiency make it a practical choice for low-cost indoor localization.

### 1.2 Contribution

- We analyzed the capacity of 915 MHz LoRa modules to perform target localization in indoor environments dedicated to electronic engineering laboratories. This was done by measuring the RSSI and calculating the mean square error between the predicted and actual target reference.
- We propose a new strategy to calculate the parameters of the RSSI-based logarithmic path loss model, specifically the path loss exponent. This strategy bypasses the traditional characterization of the RSSI measurements between LoRa-based modules and the distance.
- We determined the impact of a constant-size window in a median filter to improve location accuracy in indoor environments with 915 MHz LoRa modules.
- We demonstrated how receiver geometry and estimator weighting interact to further refine indoor localization accuracy.

### 1.3 Organization

The organization of the rest of the document is as follows. The description of the problem, the technology used, the path loss model, the trilateration algorithm, the OLS algorithm, the statistical performance, and the programming of the LoRa modules are described in Sec. 2. Section 3 presents experimental evaluations across multiple laboratory scenarios, comparing receiver geometries, unfiltered and filtered (MF/MAF) RSSI results, and OLS versus WLS performance. The final conclusions, discusses limitations, and proposes directions for future work are presented in Sec. 4.

## 2. Methodology to Lora Indoor Localization

To achieve the localization of a particular object in an indoor environment while avoiding traditional techniques that rely on correlating RSSI with distance between devices, the following summarized methodology is proposed. First, RSSI measurements are recorded from LoRa receivers $Rx_i$, see Fig. 1. Next, the location of the object is estimated using the trilateration algorithm combined with OLS by tuning the path loss exponent. So, the Mean Square Error (MSE) is then calculated to minimize the location error with respect to a known reference point. To determine the true target location, at least ten measurements were taken and averaged using a commercial stainless steel tape measure, for which the manufacturer specifies an error of 0.5 to 1 mm per meter. The reference point was consistently taken from one corner of the laboratory. This strategy provides fast tuning of the path loss parameter, as it can vary depending on the environment where the measurements are conducted. Now, it is important to describe the basic concept for implementing this methodology, which are described below.

### 2.1 LoRa Technology

The BastWAN development board is a compact, fully assembled platform designed for rapid prototyping with LoRa/LoRaWAN technology. It integrates a RAK4260 module featuring a 32-bit SAM L21 microcontroller based on the Arm Cortex-M0+ architecture that runs up to 48 MHz, offering up to 256 KB of embedded Flash and 40 KB of SRAM. The SAM L21 is engineered for ultra-low power consumption ($<$ 35 µA/MHz) and provides a rich set of peripherals including DMA, sleepwalking, an event system, up to six flexible Serial Communication Modules (SERCOMs), and up to eight timers–counters.

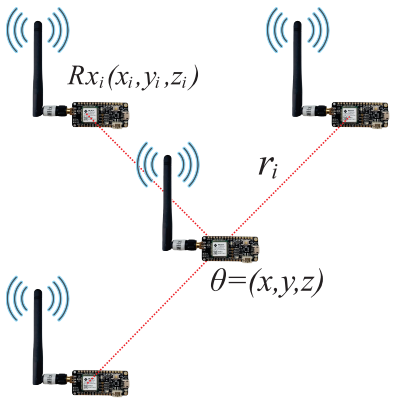


**Fig. 1.** Trilateration problem.

Its design facilitates an easy and intuitive migration between SAM L devices, with identical peripheral modules, compatible code, and a linear address map. Also, ensuring compatibility with the SAM D family of general purpose MCUs. Additionally, the board supports a wide frequency range from 862 to 1020 MHz, offers a high reception sensitivity of up to –148 dBm, and allows a maximum transmission power of 20 dBm. With native USB support, a preloaded UF2 bootloader, and compatibility with popular environments like Arduino and MakeCode, firmware updates and development are straightforward [39], [40].

In addition to its robust wireless communication capabilities, BastWAN provides versatile hardware interfaces including 20 I/O pins, multiple hardware peripherals (PWM, Serial, $I^2C$, SPI), six 12-bit analog inputs, and a 10-bit DAC output. The board also integrates a LiPo charger, a cryptographic authentication chip ATECC608A, and supports expansion for various sensors and actuators. Moreover, the SAM L21 features a full-speed USB device and embedded host, a 12-bit ADC with up to 20 channels, a dual–channel 12-bit DAC, three operational amplifiers, two analog comparators, a programmable logic block, and a Peripheral Touch Controller (PTC) for hardware touch support [41]. Available in multiple package options (QFP, QFN, and WLCSP), its open–source design and comprehensive feature set make BastWAN an ideal solution for researchers and developers working on low-power IoT applications and advanced LoRa-based projects.

## 2.2 Path Loss Model

The path loss model is a fundamental concept in wireless communication used to estimate the loss of signal strength as a function of distance between a transmitter and receiver. For LoRa devices, the path loss model based on RSSI measurements is typically described by the log-distance path loss model, which is expressed as [6]:

$$PL(d) = PL(d_0) + 10n \log_{10}\left(\frac{d}{d_0}\right) + X_\sigma. \tag{1}$$

where $PL(d)$ is expressed in dB, $d$ is the distance between the transmitter and receiver in meters, $PL(d_0)$ is the reference path loss at a close distance $d_0$, typically 1 meter. Here, $n$ is the path loss exponent, which characterizes the rate at which the signal attenuates with distance and depends on the environment. $X_\sigma$ is a random variable representing shadow fading, usually modeled as a zero-mean Gaussian random variable with standard deviation $\sigma$.

Alternatively, the RSSI received at distance $d$ can be written as:

$$RSSI(d) = P_\mathrm{t} - PL(d) \tag{2}$$

where $P_\mathrm{t}$ is the transmit power of the device in dBm [6].

Returning to the topic of path loss exponent, this is a key parameter in wireless communication models, which varies significantly across different environments. In free-space conditions, $n$ typically equals 2, representing ideal propagation with no obstructions. However, in urban areas, $n$ ranges between 2.7 and 3.5 due to obstacles such as buildings, vehicles, and other structures, which introduce reflections and shadowing. In indoor environments, $n$ can vary even more widely, ranging from 1.6 in open spaces to over 6 in densely partitioned areas such as office buildings or warehouses. These variations arise from the influence of walls, furniture, floors, and ceilings, which cause reflection, diffraction, and scattering of the signal [6].

## 2.3 Trilateration Algorithm

In this work, a basic trilateration algorithm is implemented based on Ordinary Least Squares (OLS), with equations and theory derived from the work presented in [42]. Referring to Fig. 1, let $n$ indicate the total number of measurements from all transmitters. We can define $\theta = (x, y, z)$ to represent the spatial coordinates of the target point. Now, the location of the beacon where the $i$th measurement is recorded is given by $Rx_i = (x_i, y_i, z_i)$, which is the exact location of the transmitter. Thus, the true distance can be expressed as:

$$d_i(\theta) = \sqrt{(x_i - x)^2 + (y_i - y)^2 + (z_i - z)^2}. \tag{3}$$

To ensure the location of transmitter, it is necessary to assume there are sufficient beacons so that if $\theta \neq \theta'$, then there exists at least one $i$ for which $d_i(\theta) \neq d_i(\theta')$. The variable $r_i$ denotes the measured distance from the $i$th beacon to the target point, and it can be defined as $r_i = d_i(\theta) + \epsilon_i$, where the $\epsilon_i$ are independent, with $\mathrm{E}(\epsilon_i) = 0$ and $\mathrm{var}(\epsilon_i) = \sigma^2$.

Currently, the regression formulas:

$$\begin{aligned} d_i(\theta) &= \mathrm{E}\left(r_i \mid x, y, z\right) \\ &= \sqrt{(x_i - x)^2 + (y_i - y)^2 + (z_i - z)^2} \end{aligned} \tag{4}$$

are nonlinear with respect to the unknowns $x, y, z$. However, it is possible to derive a linear regression equation, as illustrated below according to the linearization methods proposed in [43], [44].

Let $(x_r, y_r, z_r)$ represent the coordinates of an arbitrary point in $\mathbf{R}^3$, referred to as the reference point. Now, for each of the $n$ points $(x_i, y_i, z_i)$, we can express:

$$\begin{aligned} d_i(\theta)^2 = (x - x_r + x_r - x_i)^2 + (y - y_r + y_r - y_i)^2 + \ldots \\ \ldots (z - z_r + z_r - z_i)^2 . \end{aligned} \tag{5}$$

Then, the distance between the reference point and the position of the beacon where the $i$th measurement was recorded can be established as:

$$d_{ir}(\theta) = \sqrt{(x_i - x_r)^2 + (y_i - y_r)^2 + (z_i - z_r)^2}. \quad (6)$$

Let $d_r$ the distance between the reference point and the target point $(x, y, z)$, defined as

$$d_r(\theta) = \sqrt{(x - x_r)^2 + (y - y_r)^2 + (z - z_r)^2}. \quad (7)$$

To organize the information in matrix form, expanding and regrouping the terms in (5) yields:

$$\begin{aligned} 2[(x - x_r)(x_i - x_r) + (y - y_r)(y_i - y_r) + \ldots \\ (z - z_r)(z_i - z_r)] = d_r(\theta)^2 + d_{ir}^2 - d_i(\theta)^2. \end{aligned} \quad (8)$$

So, the matrix $\mathbf{X}$ and the parameter vector $\boldsymbol{\beta}$ can be defined with (9) and (10), respectively.

$$\mathbf{X} = \begin{bmatrix} 1 & 2(x_1 - x_r) & 2(y_1 - y_r) & 2(z_1 - z_r) \\ 1 & 2(x_2 - x_r) & 2(y_2 - y_r) & 2(z_2 - z_r) \\ \vdots & \vdots & \vdots & \vdots \\ 1 & 2(x_n - x_r) & 2(y_n - y_r) & 2(z_n - z_r) \end{bmatrix}, \quad (9)$$

$$\boldsymbol{\beta} = \begin{bmatrix} -d_r(\theta)^2 - \sigma^2 \\ x - x_r \\ y - y_r \\ z - z_r \end{bmatrix}. \quad (10)$$

Let $\mathbf{Y}$ denote the vector whose $i$th component is $Y_i$, which can be defined as:

$$Y_i = d_{ir}^2 - r_i^2. \quad (11)$$

Given that $d_{ir}^2$ are predetermined constants, and considering that $\mathrm{E}\left(r_i^2 | x, y, z\right) = d_i(\theta)^2 + \sigma^2$, it results in $\mathrm{E}(Y_i) = d_{ir}^2 - d_i(\theta)^2 - \sigma^2$. Therefore,

$$\mathrm{E}(\mathbf{Y}) = \mathbf{X}\boldsymbol{\beta} \quad (12)$$

where the $Y_i$ components are independent, and the next statistical relationships can be established

$$\begin{aligned} \mathrm{var}(Y_i) = \mathrm{var}(r_i^2) = \mathrm{var}\left([d_i(\theta) + \epsilon_i]^2\right) = \ldots \\ \mathrm{var}\left(2d_i(\theta)\epsilon_i + \epsilon_i^2\right) = 4d_i(\theta)^2\sigma^2 + 4d_i(\theta)\mu_3 + \mu_4 + \sigma^4 \end{aligned} \quad (13)$$

where $\sigma^2$, $\mu_3$, and $\mu_4$ are the second, third, and fourth moments of the distribution of the $\epsilon_i$, respectively.

The initial element of $\boldsymbol{\beta}$ involves a non-linear function of the components of $\theta = (x, y, z)$, indicating that this might not be a linear regression. Currently, we disregard this functional relationship and consider the first element as an independent parameter. Below, we outline a linear regression model that yields the OLS estimator of $\theta$. Given that the variances of the $Y_i$ are not uniform, this estimator may not be optimal.

### 2.3.1 The Ordinary Least Squares Estimator

To express the regression equation (12) in a linear form with respect to the unknowns $x, y, z$, it is important to note that the range of the columns of $\mathbf{X}$ is invariant to the reference point selected. Consequently, the value of $\mathbf{X}\hat{\boldsymbol{\beta}}$ remains unaffected by the reference point, implying that the estimates $\hat{x}$, $\hat{y}$, and $\hat{z}$ are also reference point independent. Therefore, it is advisable to select $\bar{\theta} = (\bar{x}, \bar{y}, \bar{z})$ as the reference point. This choice renders the last three columns of $\mathbf{X}$ orthogonal to the column of ones, allowing both the column of ones and the initial component of (10) to be excluded from the model without impacting the estimation of $\theta = (x, y, z)$.

Let $\mathbf{X}_*$ represent the matrix formed by the last three columns of (9), and define $\mathbf{Y}_*$ as $\mathbf{Y}$ plus the product of $\mathbf{X}_*$ and $\bar{\theta}$. So,

$$E(\mathbf{Y}_*) = \mathbf{X}_*\theta, \quad (14)$$

and the OLS estimator of $\theta$ can be computed as

$$\hat{\theta} = \left(\mathbf{X}_*^{\mathrm{T}}\mathbf{X}_*\right)^{-1}\mathbf{X}_*^{\mathrm{T}}\mathbf{Y}_*. \quad (15)$$

**Computational Complexity of OLS.** In this subsection we analyze the time and memory costs of the OLS-based trilateration estimator defined in (14)–(15). Let $m$ = number of receivers and $d = \dim(\theta)$, and recall that here $m = 3$ and $d = 2$. The design matrix $\mathbf{X}_*$ is therefore of size $m \times d$. For fixed parameters $m = 3$ and $d = 2$, the dominant time cost arises from the formation and solution of the normal equations in (15). In general, $T(m, d) = O\left(m\,d^2 + d^3\right)$. Specializing to $m = 3$, $d = 2$ gives $T(3, 2) = O(3 \cdot 2^2 + 2^3) = O(20) = O(1)$. Because $m$ and $d$ are fixed and small, all these costs collapse to $O(1)$ in practice.

With respect to the space complexity, storing $\mathbf{X}_*$ requires $O(m\,d)$ entries, allocating memory for $\mathbf{X}_*^{\mathrm{T}}\mathbf{X}_*$ and its inverse requires $O(d^2)$, and intermediate vectors require $O(d)$. Thus, $S(m, d) = O(m\,d + d^2)$, which yields $S(3, 2) = O(3 \cdot 2 + 2^2) = O(10) = O(1)$. Because both $m$ and $d$ are fixed and small, memory requirements are negligible in practical implementations.

## 2.4 Metrics Performance

Since the proposed heuristic localization is based on the MSE, it is necessary to define the equation as

$$MSE = \frac{1}{k}\sum_{i=1}^{k}\left(\theta - \hat{\theta}_k\right)^2 \tag{16}$$

$$= \frac{1}{k}\sum_{i=1}^{k}(x-\hat{x}_k)^2 + (y-\hat{y}_k)^2 + (z-\hat{z}_k)^2 \tag{17}$$

where $k$ is the number of measurements.

To complete the MSE, we also introduce the Root Mean Square Error (RMSE) and the Mean Absolute Error (MAE):

$$RMSE = \sqrt{MSE} = \sqrt{\frac{1}{k}\sum_{i=1}^{k}\Big[(x-\hat{x}_i)^2 + (y-\hat{y}_i)^2\Big]}, \tag{18}$$

$$MAE = \frac{1}{k}\sum_{i=1}^{k}\sqrt{(x-\hat{x}_i)^2 + (y-\hat{y}_i)^2}. \tag{19}$$

An additional metric that can corroborate the results is the Geometric Dilution of Precision (GDOP), which provides information about the influence of the relative geometry of the receivers on positioning accuracy. It is derived from the system design of multilateration or trilateration, and can be defined as in [45],

$$GDOP = \sqrt{\text{trace}\left((\mathbf{H}^{\mathrm{T}}\mathbf{H})^{-1}\right)} \tag{20}$$

where $\mathbf{H}$ is the design matrix, also known as the Jacobian of the distances with respect to the position of receiver. This expression indicates that GDOP is the square root of the trace of the inverse of $\mathbf{H}^{\mathrm{T}}\mathbf{H}$, which reflects how the spatial configuration of receivers affects positioning accuracy. The GDOP parameter is intended to be as low as possible, it is widely accepted in the technical literature that a value below 2 is an excellent geometry.

The purpose of these basic metrics is to establish the known parameters based on the literature and to adjust them in order to achieve optimal performance.

### 2.4.1 LoRa Module Programming

The code of Arduino, described in Algorithm 1, demonstrates a basic example of a LoRa transmitter, utilizing the SPI and LoRa libraries to wirelessly send a sequence of incrementing numbers via the LoRa protocol. The code begins with initialization, where serial communication is started for debugging and monitoring, and specific GPIO pins are configured for the LoRa module and built-in LED. The LoRa module is then set up at a frequency of 915 MHz, with its spreading factor and signal bandwidth configured to control modulation and transmission quality.

For this test, the Spreading Factor (SF) was set to 7, with a bandwidth of 125 kHz, a Coding Rate (CR) of 4/5, and a transmission power of 17 dBm, approximately 50.12 mW. In the main loop, the code transmits a packet containing the current counter value, with a built-in LED indicating activity during transmission. The counter increments with each loop iteration, and delays are incorporated to pace the transmissions. This code is ideal for testing LoRa communication, verifying proper transmitter functionality, and debugging the setup with both visual and serial feedback. The configuration parameters can be summarized in the Tab. 1.

**Algorithm 1.** LoRa transmitter code algorithm.

**Input:** LoRa module pins, transmission frequency, spreading factor, bandwidth
**Output:** Periodic LoRa packets with incrementing counter
**Require:** LoRa module is properly connected and configured
**Ensure:** Transmissions occur without errors
Initialize SPI and LoRa libraries
Declare `counter` and set it to 0
Start serial communication at 9600 baud
**print** "LoRa Sender" to the serial monitor
Configure GPIO pins for the LoRa module and LED
Initialize LoRa module at 915 MHz
Configure LoRa spreading factor and signal bandwidth
**loop**
  **print** Current `counter` to the serial monitor
  Turn on the built-in LED
  Begin a LoRa packet
  Set switch pin to low
  Add `counter` value to the packet
  End LoRa packet transmission
  Increment `counter`
  Wait for 500 ms
  Turn off the built-in LED
  Wait for another 500 ms
**end loop**
**return** Success of transmission

| Parameter | Value |
|---|---|
| Operating frequency | 915 MHz |
| Spreading Factor (SF) | 7 |
| Bandwidth (BW) | 125 kHz |
| Coding Rate (CR) | 4/5 |
| Transmit power | 17 dBm (≈50.12 mW) |

**Tab. 1.** LoRa module configuration parameters.

The LoRa Receiver Code, which is shown in Algorithm 2, initializes the SPI and LoRa libraries, configures the RF switch for receiving mode, and sets the LoRa module with a frequency of 915 MHz, a SF of 7, and a signal bandwidth of 125 kHz. The code continuously checks for incoming packets and, upon detection, reads the data byte by byte, appends it to a string, and prints the received message along with its RSSI to the serial monitor. This ensures reliable reception and monitoring of LoRa transmissions while handling data parsing and display efficiently. Also, in Algorithm 2, it is possible to appreciate an infinite loop, which is used as a safety mechanism to stop execution if LoRa initialization fails, preventing undefined behavior and notifying the user to correct the issue. This ensures that the receivers do not operate without a valid communication link, there by maintaining system reliability.

**Algorithm 2.** LoRa receiver code algorithm.

**Input:** LoRa module pins, receiving frequency, spreading factor, bandwidth
**Output:** Received LoRa packets with signal strength (RSSI)
**Require:** LoRa module is properly connected and configured
**Ensure:** Received packets are displayed correctly on the serial monitor
Initialize SPI and LoRa libraries
Start serial communication at 9600 baud
**print** "LoRa Receiver" to the serial monitor
Set RF switch pin as OUTPUT
Set RF switch to HIGH (receiver mode)
Configure LoRa module pins: `SS`, `RFM_RST`, `RFM_DIO0`
Initialize LoRa module at 915 MHz
**if** LoRa initialization fails **then**
  **print** "Starting LoRa failed!" to the serial monitor
  Enter infinite loop
**end if**
Configure LoRa spreading factor to 7
Set LoRa signal bandwidth to 125 kHz
**loop**
  Parse for incoming LoRa packets
  **if** a packet is received **then**
    Initialize empty string `incoming`
    **while** LoRa has available data **do**
      Read one byte and append to `incoming`
    **end while**
    Print `incoming` message to the serial monitor
    Print RSSI value to the serial monitor
    Print a tab separator `\t`
    Print RSSI value again for clarity (optional)
    Print a newline character
  **end if**
**end loop**
**return** Successful packet reception and RSSI display

# 3. Results

## 3.1 Finding Path Loss Exponent

Aiming to find an optimal level for the path loss exponent, several experiments in different scenes were realized by tuning the value of $n$ in (1) and analyzing the MSE of estimated position with respect to the true location of the transmitter. According to the literature [6], [46], the path loss exponent recommended for indoor environments ranges from $n = 1.6$ to $n = 1.8$. However, in obstructed buildings, it can achieve values between $n = 4$ to $n = 6$. For an exhaustive search, we propose to employ a range from $n = 2$ to $n = 6$ to find the minimal MSE, according to different environments.

To carry out our studies, three different scenarios were selected within the same building to evaluate wireless transmission performance specifically under Line of Sight (LOS) conditions in indoor environments. The indoor measurements were conducted in Building B of the Engineering Department at the Universidad Autónoma de Zacatecas, Jalpa Campus, in Mexico. Here, RSSI levels were measured by placing the transmitter (TX) and receiver (RX) modules on worktables commonly used in these spaces, which allowed positioning the modules at a height of 0.74 meters. This setup aimed to conduct experiments in a realistic, simple, and natural environment without the need for sophisticated mounting equipment. During the measurements, environmental factors, such as temperature and humidity, were considered negligible, and there was minimal human movement in the indoor spaces under study.

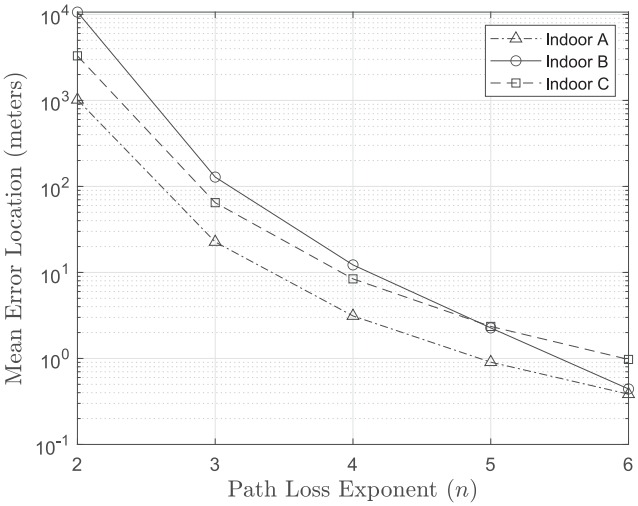


**Fig. 2.** Mean error location evolution in meters by tuning the path loss exponent $n$.

In Fig. 2, the evolution of the mean localization error is shown when adjusting the value of the path loss exponent $n$ for the different scenes. The performance of errors is similar, achieving the maximum error at $n = 2$ and the minimum error at $n = 6$. The minimal mean errors obtained in the Power Electronics, Digital Electronics, and Network Laboratories were 0.3842 m, 0.4419 m, and 0.9732 m, respectively.

From the path loss exponent tuning experiments, the optimal exponent can be established as $n = 6$ for all the environments, aligning with literature values for obstructed indoor environments. The fitted exponent minimize localization error as shown in Fig. 2, with residual analysis indicating log-normal shadowing assumptions hold reasonably well within the tested range. Based on these results, it is possible to analyze each scene individually with the path loss that generates the minimum error.

## 3.2 Indoor A: Power Electronics Laboratory

The first set of measurements was conducted in the Power Electronics Laboratory at the Jalpa Campus. The laboratory has an approximate area of 80 square meters and is constructed of concrete with brick walls painted white. The ceiling is also made of concrete and painted in a light color. Following the cardinal guidance, in the far-right corner, there is power electronics equipment, including motors and generators, thyristor and IGBT transistor modules, three-phase power supplies, cabinets with PLCs, and a conveyor belt is also installed. The room has two windows, six computers, and three rows of chairs and tables in the center. Another row of tables is located at the back, directly in front of the room.

Figure 3(a) shows the actual experimental environment in the Power Electronics Laboratory, while Fig. 3(b) presents its layout schematic. Due to free space and arrangement of laboratory furniture, the TX was arbitrary located in coordinates in $x = 3.88$ m and $y = 4.87$ m taken as origin reference the southwest corner. Likewise, the receivers are placed at $(x_1 = 8.74, y_1 = 1)$, $(x_2 = 1, y_2 = 1)$, and $(x_3 = 1, y_3 = 6.76)$, for $Rx_1$, $Rx_2$, and $Rx_3$, respectively. In Fig. 3(b), the black, blue, and red points indicate the arbitrary positions where the RX nodes were installed, while the TX node is represented by a blue triangle indicating its placement. The blue circles represent the location estimated based on 300 RSSI measurements and the OLS algorithm. The gray dotted circles are drawn by using the mean of RSSI measurements and computing the distance with (3). The red cross shows the mean of positions estimated of TX, showing that the position of TX is located at center of the room.

The measurements taken for each receiver in the Electronic Power Laboratory are shown in Fig. 4. For Receiver 1 ($Rx_1$), the maximum and minimum values were –59 dBm and –68 dBm, respectively, with a median of −66 dBm. For Receiver 2 ($Rx_2$), the maximum value was –60 dBm, the minimum was –71 dBm, and the median was −67 dBm. For the third receiver ($Rx_3$), the highest, lowest, and median values were −59 dBm, −70 dBm, and −68 dBm, respectively. Some peaks can be observed across the three receivers, which might be caused by interference from other devices. However, a stable median is evident, enabling accurate location approximation based on the trilateration algorithm.

Once the location of the Transmitter is estimated, MSE with respect to the reference coordinates, which are well-known, is calculated. The error for each measurement is illustrated in Fig. 5. In this graph, some error values on the order of $10^{-15}$ can be observed. This level of accuracy is achieved when the three Receiver measurements are similar. For example, for the measurement $k = 43$, the receivers $Rx_1$, $Rx_2$, and $Rx_3$ each registered an RSSI value of −67 dBm. Consequently, the MSE at $k = 43$ in Fig. 5 was $1.2 \times 10^{-15}$ m.

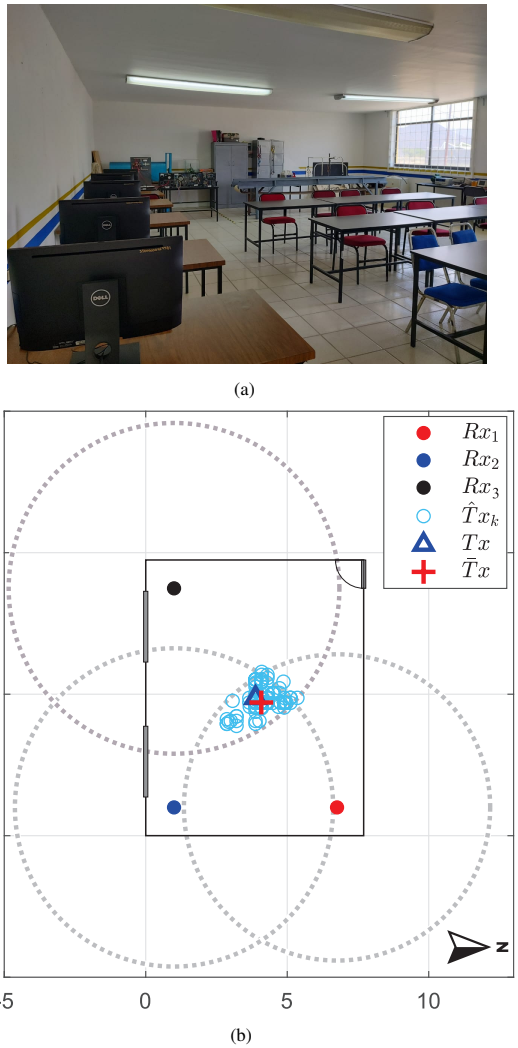


Fig. 3. (a) Real environment in Power Electronics Laboratory; (b) Estimation of transmitter location in Power Electronics Laboratory.

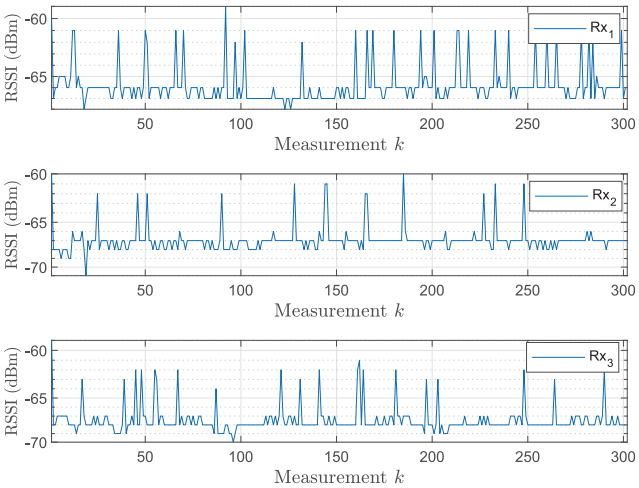


**Fig. 4.** RSSI levels of three receivers for 300 measurements in Power Electronics Laboratory.

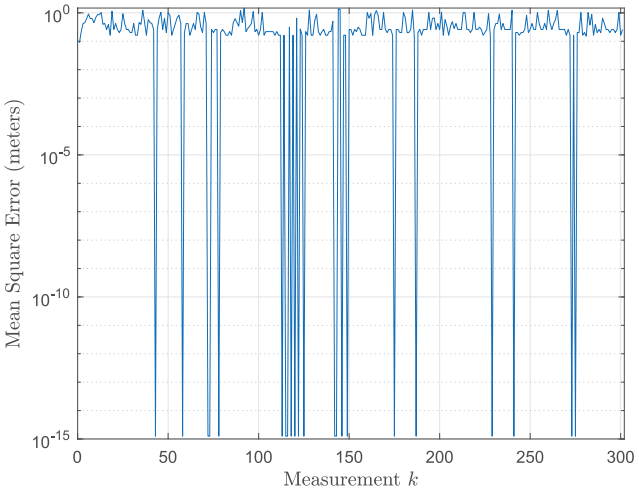


**Fig. 5.** Mean square error of estimated location in Power Electronics Laboratory.

### 3.3 Indoor B: Network Laboratory

The second set of measurements was conducted in the Network Laboratory at the Jalpa Campus. This room has the same dimensions and construction materials as the previous one, however, the furniture and equipment are different. Following the cardinal orientation, in the top-right corner near $Rx_1$, there is a 48-port switch, routers, modems, a desktop computer, and a wooden desk. In the center of the laboratory, there are 8 networked computers connected with UTP cables over wooden desks. In the bottom-left corner, near $Rx_3$, there are storage racks for tools and networking equipment.

Figures 6(a) and (b) depict the real experimental setup and layout schematic in Network Laboratory, respectively. Given the available open space and the arrangement of the furniture, the transmitter (TX) was positioned arbitrarily at coordinates $x = 3.89$ m and $y = 4.87$ m, using the southwest corner as the origin. Similarly, the receivers were located at $(x_1 = 6.78, y_1 = 1)$, $(x_2 = 1, y_2 = 1)$, and $(x_3 = 1, y_3 = 8.74)$ meters for $Rx_1$, $Rx_2$, and $Rx_3$, respectively. In Fig. 6(b), the black, blue, and red markers denote the specific positions where the RX nodes were deployed, while the TX node is depicted by a blue triangle indicating its placement. The blue circles represent the estimated positions based on 300 RSSI measurements processed using the OLS algorithm. Additionally, gray dashed circles are shown, which were calculated using the average RSSI values and the distance formula from (3). The red cross signifies the average of the estimated TX positions, highlighting that the transmitter's location is approximately at the center of the room.

Figure 7 displays the data collected for each receiver in the Network Laboratory, with a total of 300 measurements taken for each receiver. For Receiver 1 ($Rx_1$), the signal strength reached a maximum of –57 dBm and a minimum of –81 dBm, with a median value of −74 dBm. Receiver 2 ($Rx_2$) recorded a maximum of –58 dBm, a minimum of –72 dBm, and a median of −65 dBm. Similarly, Receiver 3 ($Rx_3$) had a peak value of −51 dBm, a minimum of −70 dBm, and a median of −65 dBm. As observed in previous experiments, peaks in the measurements of the three receivers are likely caused by interference from other electronic devices. Despite these anomalies, the median values remain consistent, allowing the trilateration algorithm to provide an accurate estimation of location.

To analyze the estimated location of the transmitter $Tx$, the MSE is calculated using the actual reference coordinates of the transmitter. The error for each measurement is shown in Fig. 8. The minimal error observed is 0.1401 m, while the maximum error is 3.5373 m. The accuracy level in this experiment is notably lower than that achieved in the Power Electronics scene, likely due to the lack of synchronization between RSSI measurements from the receivers. However, the median location error is 0.8448 m, which is reasonable and allows us to infer that the receiver is within the indoor environment.

(a)

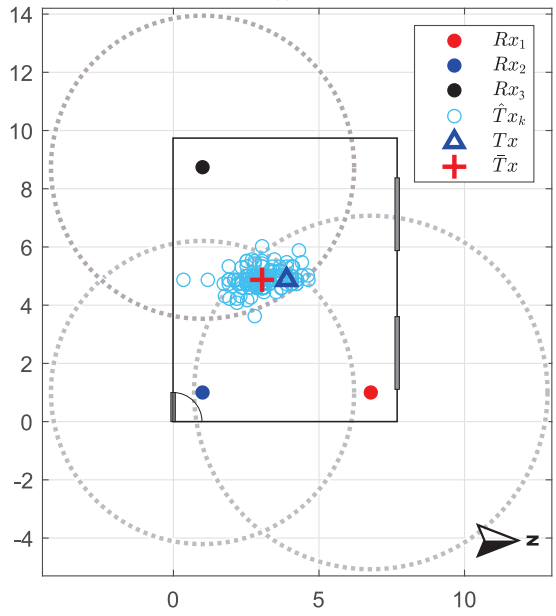


(b)

Fig. 6. (a) Real environment in Network Laboratory; (b) Estimation of transmitter location in Network Laboratory.

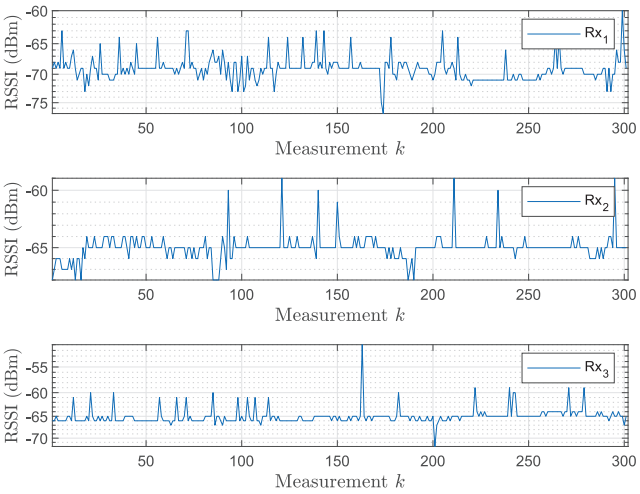


**Fig. 7.** RSSI levels of three receivers for 300 measurements in Network Laboratory.

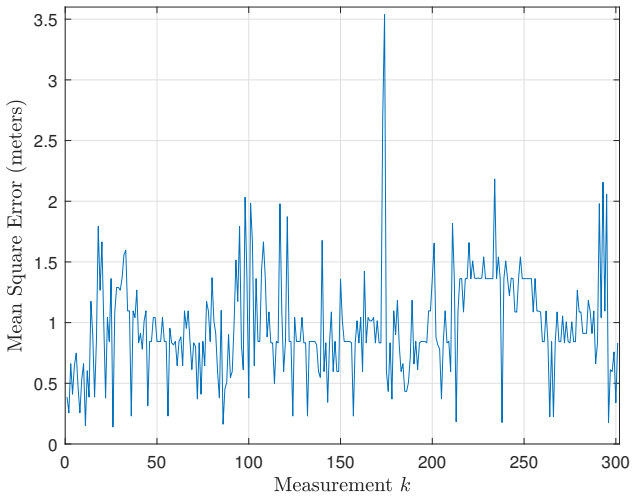


**Fig. 8.** MSE of estimated location in Network Laboratory.

## 3.4 Indoor C: Digital Electronics Laboratory

The third set of measurements was carried out in the Digital Electronics Laboratory, located in the same building. This room shares the same dimensions and construction materials as the previous one. Following the cardinal orientation, laboratory tables equipped with desktop computers, multimeters, power supplies, oscilloscopes, robotic kits, and independent power sources are positioned along the east and west walls near the windows. In the center of the laboratory, there are 12 wooden desks with chairs. In the bottom-left corner, near $Rx_3$, storage racks are present for tools and electronic equipment. For this test, it is proposed to reduce the measurements by a factor of five to verify the accuracy of the location with fewer samples than in the previously described experiment.

Figure 9(a) depicts the actual experimental setup in the Digital Electronics Laboratory, while Fig. 9(b) illustrates the corresponding layout schematic. The transmitter ($Tx$) was placed at coordinates $x = 4$ m and $y = 4$ m, with the southwest corner acting as the origin. The receivers were positioned as follows: $Rx_1$ at ($x_1 = 7.03$, $y_1 = 1.5$), $Rx_2$ at ($x_2 = 0.7$, $y_2 = 1.5$), and $Rx_3$ at ($x_3 = 1$, $y_3 = 8.67$) meters. In Fig. 9(b), the black, blue, and red markers indicate the exact locations of the RX nodes, while the TX node is represented by a blue triangle to show its placement. The blue circles depict the estimated positions, where the RSSI measurements were reduced to $k = 61$ for processing using the OLS algorithm. As in previous experiments, gray dashed circles are included, calculated based on the mean RSSI values and the distance formula from (3). The red cross represents the average of the estimated TX positions, emphasizing that the transmitter is located approximately at the center of the room.

Figure 10 presents the signal strength data gathered for each receiver in the Digital Electronics Laboratory. In this figure, 62 samples appear, the last one corresponds to the median of the samples. Receiver 1 ($Rx_1$) recorded a maximum signal of –65 dBm, a minimum of –73 dBm, and a median

(a)

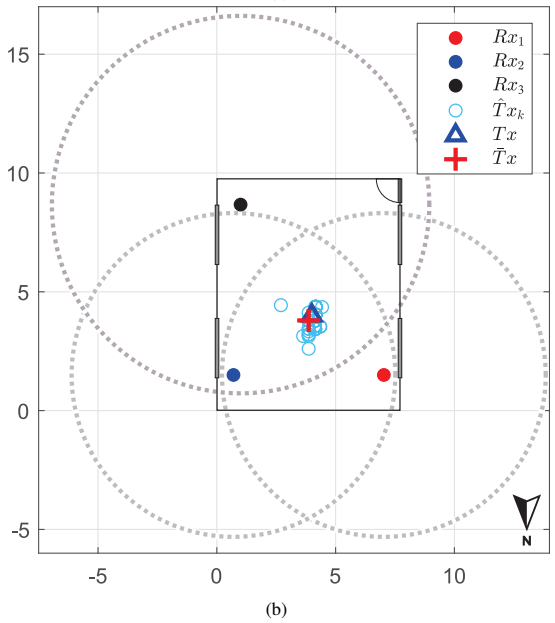


(b)

Fig. 9. (a) Real environment in Digital Laboratory; (b) Estimation of transmitter location in Digital Laboratory.

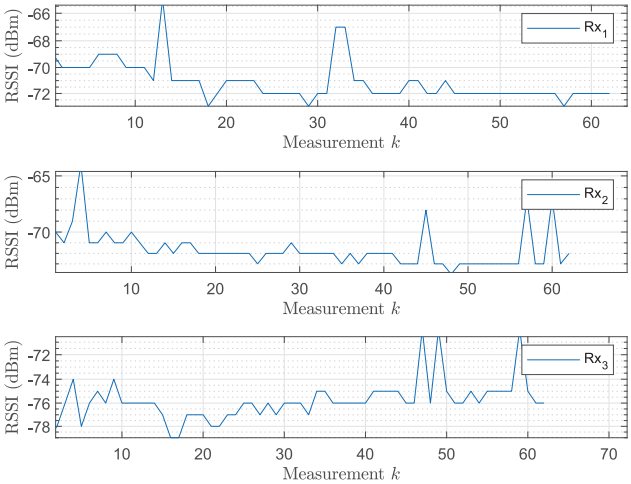


**Fig. 10.** RSSI levels of three receivers for 61 measurements in Digital Electronics Laboratory.

of −72 dBm. Similarly, Receiver 2 ($Rx_2$) reached a peak of –64 dBm, a low of –74 dBm, and a median value of −72 dBm. In contrast, Receiver 3 ($Rx_3$) had a maximum strength of −70 dBm, a minimum of −79 dBm, and a me-

dian of −76 dBm. Although occasional peaks were observed in the measurements for the second and third receivers, the trilateration algorithm was still able to provide an accurate estimation of the location of the transmitter.

Figure 11 illustrates the MSE for each measurement conducted in the Digital Electronics Laboratory to estimate the transmitter's position. The lowest error recorded was 0.1629 m, while the highest error reached 1.8165 m. Although the accuracy in this experiment is lower than that achieved in the Power Electronics setup, it surpasses the error levels observed in the Network Laboratory. Notably, the median error was 0.5566 m, which is sufficient to confirm that the transmitter is positioned within the indoor environment.

As a statistical criterion, confidence intervals were computed from the RSSI measurements. In this study, 95% confidence limits were obtained for each set of RSSI measurements collected in three different laboratory environments. In the Power Laboratory, the RSSI values ranged as follows $Rx_1$ from –66.02 to –65.64 dBm, $Rx_2$ from –67.10 to –66.79 dBm, and $Rx_3$ from –67.63 to –67.27 dBm. In the Network Laboratory, the intervals were $Rx_1$ from –69.36 to –68.91 dBm, $Rx_2$ from –65.13 to –64.87 dBm, and $Rx_3$ from –65.23 to –64.85 dBm. Finally, the Digital Laboratory showed $Rx_1$ between –71.49 and –70.73 dBm, $Rx_2$ between –72.11 and –71.23 dBm, and $Rx_3$ between –76.28 and –75.39 dBm. The average results indicate that RSSI measurements were stronger in the Power and Network Laboratories compared to the Digital Laboratory, suggesting potentially greater signal attenuation or interference in the latter environment. The relatively narrow confidence intervals of all scenes suggest good quality measurement. It is worth mentioning that the outliers were not removed or given special treatment, in order to preserve the signals in their original form before applying any filtering stage. The computed GDOP values are 1.2621 for the Power Laboratory, 1.3458 for the Network Laboratory, and 1.2160 for the Digital Laboratory. These levels indicate a favorable geometry of receivers in all locations, supporting reliable positioning accuracy. Computed GDOP values correlate strongly with measured localization errors, validating GDOP as a predictive metric. In low GDOP configurations, error dispersion decreases, supporting its use in the strategic planning of receiver placement.

Specific analysis of environment revealed that the Power Electronics Laboratory exhibited higher RSSI variability probably due to metallic surfaces and equipment, while the Network Laboratory showed increased interference from active network devices. The Digital Electronics Laboratory, with fewer reflectors, yielded more stable measurements. The reduction in the number of measurement samples in the Digital Electronics Laboratory environment was proposed based on the premise that a real-time localization system should be able of estimating the position of a moving object or person within an enclosed space. The decision to decrease the number of samples confirmed that localization error increases as sample count decreases, however, the resulting error remains within acceptable bounds. In particular, the estimated target position remains sufficiently accurate to determine whether it is located within the room boundaries.

To gain a broader understanding of how the number of samples influences the localization error, a brief analysis was conducted using the theoretical equation $\sigma/\sqrt{n}$, where $\sigma$ and $n$ represents the standard deviation and the number of samples, respectively. Additionally, a Monte Carlo simulation was performed using the standard deviation of the measurements and 1000 trials under Gaussian noise conditions, considering several sample window sizes 10, 30, 120, 300, and 600. Figure 12 presents the results of this analysis, highlighting latency measurements and the mean error standard deviation of RSSI in dBm.

Here, the standard error of the mean for 300 samples is given by the expression $\sigma/\sqrt{300}$. It is noteworthy that even when the measurement window is doubled, the improvement in standard error is marginal, approximately 0.0338.

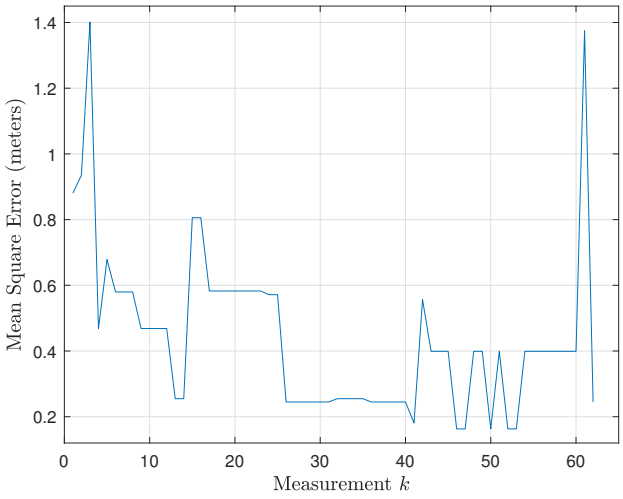


**Fig. 11.** MSE of estimated location in Digital Electronics Laboratory.

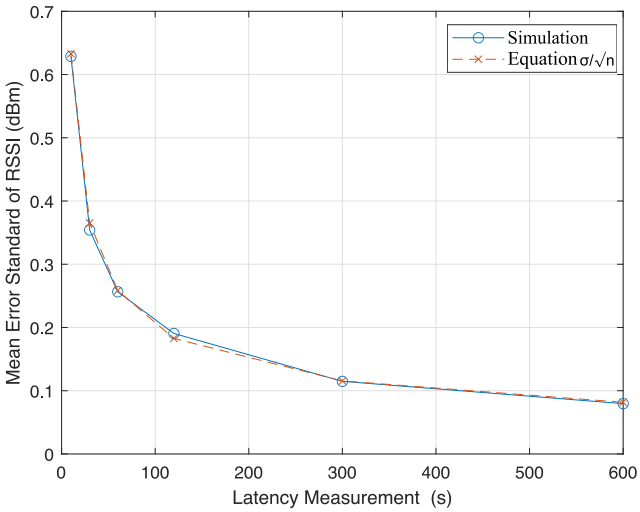


**Fig. 12.** Latency measurement versus mean error standard of RSSI [dBm].

### 3.5 Comparison by Filtered RSSI

Aiming to improve the accuracy of the location of transmitter, it is proposed to implement a MF to process the RSSI measurements. Due to the presence of peaks in RSSI measurements caused by multipath propagation from devices, the MF was chosen. The median filter is a non linear digital filtering technique often used to remove noise from signals by replacing each data point with the median value of its surrounding neighbors [47]. An odd window size is essential for the filter to ensure a defined median value, preserving important features like edges while effectively reducing noise. Additionally, a performance comparison using a MAF [48] was carried out to highlight differences in the estimated location based on the metrics described in Sec. 2.4. The MAF is theoretically preferred because of its robustness against outliers and abrupt changes in signal amplitude.

To this stage, the window sizes $W_n$ of 1, 3, 5, 7, 11, 23, 29, and 41 were selected to evaluate the performance of both MF and MAF over a range of smoothing intensities. The selected window sizes follow a quasi–logarithmic progression, allowing for efficient analysis of filtering effects at multiple scales without exhaustive testing of all possible sizes. Smaller windows are employed to retain fine details while reducing high frequency noise, whereas larger windows are used to assess the ability of filters to suppress trends and low frequency components. The window size of 1 serves as a baseline, representing the unfiltered signal for comparative purposes. Table 2 presents the MSE for the various proposed laboratories. Here, the symbols ↓ and ↑ highlight the minimum and maximum error values, respectively.

In comparison with the results obtained without applying the MF and MAF, or with filters using a window size of one, Table 2 demonstrates a reduction in error across all scenarios. For the Power Electronics Laboratory, an error reduction of 0.4655 m was achieved with window sizes $W_n = 7$ and $W_n = 11$. While the MAF achieved its best error reduction of 1.0067 m when using a window size of $W_n = 41$. Additionally, the experiments conducted in the Network Laboratory achieved the most significant improvement, with an error reduction of 2.1749 m for the MF using window sizes $W_n = 23$ and $W_n = 29$. For the MAF, in the same environment, the error decreased by 2.1953 m when using a window size of $W_n = 41$. Furthermore, in the Digital Electronics Laboratory, an accuracy improvement of 0.4418 m and 1.0719 m was observed for the MF with a window size of $W_n = 29$, and for the MAF with $W_n = 41$, respectively.

Based on the results in Tab. 2, it is recommended to employ a MF with a window size of $W_n = 7$ for the experiments described previously. This recommendation is based on several factors. First, the error differences compared to the best results for the three scenarios are 0 m, 0.0071 m, and 0.188 m, respectively. Second, the selected window size is small, which helps minimize computational requirements for hardware processing. Additionally, $W_n = 5$ can also be considered, however, the accuracy differences compared to the best results indicate it performs slightly worse. Although all experiments were conducted under similar Line of Sight (LoS) conditions, the layout and equipment in each laboratory is different. In the Power and Network Labs, the estimation error differed by only 0.007 m. By contrast, the Digital Electronics Lab, where just 61 RSSI samples were collected, showed a much larger variation. This emphasizes how a limited sample size can degrade localization accuracy.

Regarding the MAF, the smallest differences in error are observed between window sizes $W_n = 5$, $W_n = 7$, and $W_n = 11$, with slightly higher differences occurring between $W_n = 23$ and $W_n = 29$. This behavior is the same across the different scenes. Therefore, as a preliminary deduction, it is recommended to use a window size of $W_n = 5$, $W_n = 7$, or $W_n = 11$ for the MAF to reduce location estimation error. However, if the goal is to maximize estimation accuracy and computational cost is not a limiting factor, a window size greater than $W_n = 29$ is recommended.

It is worth mentioning that, although the MAF appears to outperform the MF by a significant difference, this observation is based only on maximum error values. Therefore, a more general and detailed comparison is required. This evaluation is carried out using the MSE, RMSE, and MAE metrics described in Sec. 2.4. The localization errors estimated in the Power Laboratory using several window sizes $W_n$ for both the median filter and the Moving median filter are presented in Tab. 3. As shown, there is only a minimal difference between the results obtained by both filters for $W_n = 5$, $W_n = 7$, and $W_n = 11$ across all metrics. Overall, the median filter yields better results for most window sizes, except for $W_n = 41$, where the MAF performs slightly better. This suggests that the MAF requires a larger window size to outperform the median filter for the Power Laboratory environment.

| Window $W_n$ | **Maximum median filter error** | | |
|---|---|---|---|
| | Pow. Elec. Lab | Net Lab. | Dig. Elec. Lab |
| 1 | 1.4785 ↑ | 3.5372 ↑ | 1.8165 ↑ |
| 3 | 1.3663 | 2.6985 | 1.6728 |
| 5 | 1.0261 | 1.6648 | 1.4014 |
| 7 | 1.0130 ↓ | 1.3694 | 1.5627 |
| 11 | 1.0130 ↓ | 1.3694 | 1.5627 |
| 23 | 1.2042 | 1.3623 ↓ | 1.4764 |
| 29 | 1.2042 | 1.3623 ↓ | 1.3747 ↓ |
| 41 | 1.0130 | 1.3623 | 1.1168 |
| $W_n$ | **Maximum moving average filter error** | | |
| 1 | 1.4785 ↑ | 3.5372 ↑ | 1.8165 ↑ |
| 3 | 0.9724 | 2.2168 | 1.5009 |
| 5 | 0.7716 | 1.6558 | 1.2853 |
| 7 | 0.7287 | 1.5257 | 1.2853 |
| 11 | 0.6804 | 1.4858 | 1.1112 |
| 23 | 0.5745 | 1.4265 | 0.7533 |
| 29 | 0.5346 | 1.3533 | 0.7533 |
| 41 | 0.4718 ↓ | 1.3419 ↓ | 0.7446 ↓ |

**Tab. 2.** Maximum mean square errors in meters based on the implementation of MF and MAF with several windows $W_n$.

| $W_n$ | Median filter | | | Moving average filter | | |
|---|---|---|---|---|---|---|
| | MSE | RMSE | MAE | MSE | RMSE | MAE |
| 1 | 0.2491 | 0.4991 | 0.3841 | 0.2491 | 0.4991 | 0.3841 |
| 3 | 0.1265 | 0.3556 | 0.2875 | 0.1512 | 0.3888 | 0.3394 |
| 5 | 0.0806 | 0.2839 | 0.2554 | 0.1189 | 0.3449 | 0.3104 |
| 7 | 0.0766 | 0.2767 | 0.2494 | 0.1046 | 0.3235 | 0.2921 |
| 11 | 0.0703 | 0.2652 | 0.2434 | 0.0904 | 0.3006 | 0.2747 |
| 23 | 0.0730 | 0.2703 | 0.2518 | 0.0762 | 0.2760 | 0.2587 |
| 29 | 0.0679 | 0.2607 | 0.2456 | 0.0734 | 0.2710 | 0.2554 |
| 41 | 0.0731 | 0.2705 | 0.2493 | 0.0688 | 0.2623 | 0.2500 |

**Tab. 3.** Power laboratory location mean square error, root mean square error, and mean absolute error to a median filter and moving average filter with several windows $W_n$.

| $W_n$ | Median filter | | | Moving average filter | | |
|---|---|---|---|---|---|---|
| | MSE | RMSE | MAE | MSE | RMSE | MAE |
| 1 | 1.1312 | 1.0635 | 0.9732 | 1.1312 | 1.0635 | 0.9732 |
| 3 | 0.9962 | 0.9981 | 0.9396 | 0.9714 | 0.9856 | 0.9183 |
| 5 | 0.9351 | 0.9670 | 0.9260 | 0.9226 | 0.9605 | 0.9052 |
| 7 | 0.9183 | 0.9583 | 0.9182 | 0.8965 | 0.9468 | 0.8992 |
| 11 | 0.9036 | 0.9505 | 0.9123 | 0.8680 | 0.9316 | 0.8939 |
| 23 | 0.8909 | 0.9438 | 0.9161 | 0.8362 | 0.9144 | 0.8893 |
| 29 | 0.8746 | 0.9352 | 0.9111 | 0.8278 | 0.9098 | 0.8889 |
| 41 | 0.8862 | 0.9414 | 0.9197 | 0.8164 | 0.9035 | 0.8885 |

**Tab. 4.** Network laboratory location mean square error, root mean square error, and mean absolute error to a median filter and moving average filter with several windows $W_n$.

| $W_n$ | Median filter | | | Moving average filter | | |
|---|---|---|---|---|---|---|
| | MSE | RMSE | MAE | MSE | RMSE | MAE |
| 1 | 0.7375 | 0.8587 | 0.6838 | 0.7375 | 0.8587 | 0.6838 |
| 3 | 0.4448 | 0.6670 | 0.5308 | 0.4438 | 0.6662 | 0.5725 |
| 5 | 0.2589 | 0.5088 | 0.4418 | 0.3561 | 0.5967 | 0.5139 |
| 7 | 0.2967 | 0.5447 | 0.4655 | 0.3210 | 0.5666 | 0.4925 |
| 11 | 0.2818 | 0.5308 | 0.4560 | 0.2648 | 0.5146 | 0.4612 |
| 23 | 0.2760 | 0.5254 | 0.4530 | 0.2115 | 0.4599 | 0.4120 |
| 29 | 0.2302 | 0.4798 | 0.4007 | 0.2040 | 0.4517 | 0.3951 |
| 41 | 0.1681 | 0.4101 | 0.3407 | 0.1689 | 0.4110 | 0.3393 |

**Tab. 5.** Digital laboratory location mean square error, root mean square error, and and mean absolute error to a median filter and moving average filter with several windows $W_n$.

| | $W_n$ | Median filter | | | Moving average filter | | |
|---|---|---|---|---|---|---|---|
| | | MSE | RMSE | MAE | MSE | RMSE | MAE |
| **Reference 1** $Tx_{\text{ref1}}$ | 1 | 1.112 | 1.054 | 1.019 | 1.112 | 1.054 | 1.019 |
| | 3 | 1.077 | 1.038 | 1.025 | 1.040 | 1.020 | 1.003 |
| | 5 | 1.076 | 1.037 | 1.033 | 1.020 | 1.010 | 0.999 |
| | 7 | 1.084 | 1.041 | 1.039 | 1.010 | 1.005 | 0.997 |
| | 11 | 1.102 | 1.050 | 1.048 | 1.000 | 1.000 | 0.995 |
| | 23 | 1.102 | 1.050 | 1.049 | .990 | 0.995 | 0.993 |
| | 29 | 1.136 | 1.066 | 1.065 | 0.989 | 0.995 | 0.993 |
| | 41 | 1.145 | 1.070 | 1.068 | 0.989 | 0.994 | 0.994 |
| **Reference 2** $Tx_{\text{ref2}}$ | 1 | 0.720 | 0.848 | 0.805 | 0.720 | 0.848 | 0.805 |
| | 3 | 0.682 | 0.826 | 0.789 | 0.540 | 0.735 | 0.665 |
| | 5 | 0.683 | 0.826 | 0.790 | 0.497 | 0.705 | 0.637 |
| | 7 | 0.665 | 0.816 | 0.780 | 0.474 | 0.689 | 0.630 |
| | 11 | 0.670 | 0.819 | 0.786 | 0.450 | 0.671 | 0.618 |
| | 23 | 0.681 | 0.825 | 0.794 | 0.420 | 0.648 | 0.615 |
| | 29 | 0.686 | 0.828 | 0.798 | 0.415 | 0.644 | 0.615 |
| | 41 | 0.693 | 0.833 | 0.804 | 0.408 | 0.639 | 0.614 |

**Tab. 6.** Power laboratory location moving the target MSE, RMSE, and MAE to a median filter and moving average filter with several windows $W_n$.

The metrics computed in the Network Laboratory are presented in the Tab. 4. The results demonstrate that the MAF uniformly outperforms the MF across all window sizes $W_n$, particularly for larger windows. Although both filters decrease localization errors as $W_n$ increases, the MAF achieves lower MSE, RMSE, and MAE values. This performance can be attributed to the nature of RSSI measurements, which typically exhibit continuous, Gaussian-like noise rather than impulsive outliers. Consequently, the MAF is more effective to smoothing these fluctuations and preserving signal trends, improving its effectiveness for RSSI based localization in this experimental setting.

Finally, Table 5 also compares the MF and the MAF across window sizes $W_n$. At $W_n = 1$, both filters are identical since no smoothing is applied. For all windows, the MAF yields slightly lower MSE, RMSE, and MAE, indicating a moderate advantage in more precise filtering. However, beginning at $W_n = 11$, the MAF demonstrates a modest advantage, after which it clearly surpasses the MF, reaching a lower MSE, RMSE, and MAE value, and this difference increases for larger windows $W_n = 23$ and $W_n = 29$. These results suggest that while the MF is more suitable for small window sizes effectively reducing sporadic outliers, the performance of MAF improves through leveraging the continuous, Gaussian-like nature of RSSI noise, resulting in smoother and more precise location estimates.

We note that the choice of a fixed window size $W_n$ for the MF and MAF was guided entirely by empirical evaluation rather than analytical derivation. In particular, window lengths from $W_n = 5$ to $W_n = 9$ samples consistently minimized MSE, RMSE, and MAE for static transmitter. This conclusion is based on the results presented in Tabs. 2–5. However, this optimal range could vary in response to substantially different noise distributions, sampling rates, or beacon geometries. Moving average filtering consistently outperformed median filtering in reducing localization error, particularly for window sizes between 5 and 11. Statistical metrics confirm these improvements and indicate that a window size of 7 achieves an effective balance between smoothing and responsiveness. Furthermore, computational benchmarks suggest that this configuration is feasible for real time implementation on embedded hardware.

## 3.6 Modified Geometry and Comparison with WLS

To support our proposed methodology, we designed an additional receiver geometry and defined two new reference positions in the Power Electronics Laboratory. The receiver positions are now located at $Rx_1$ at (6.74, 2), $Rx_2$ at (0.3, 4.87), and $Rx_3$ at (7.44, 8.74). The first reference position $Tx_{\text{ref1}}$ was placed at (3.87, 2.5), and the second $Tx_{\text{ref2}}$ at (3.87, 6.5). In Tab. 6, the MSE, RMSE, and MAE metrics for each reference are shown using different windows $W_n$ for the MF and MAF filters.

For $Tx_{\text{ref1}}$, an increase in error is observed compared to previous experiments in the same environment. This may be due to the proximity of the first and second receivers, $Rx_1$ and $Rx_2$, to the transmitter. However, the small differences in error for $W_n = 5$, 7, and 11 remain consistent across MSE, RMSE, and MAE. For $Tx_{\text{ref2}}$, the error decreases compared to $Tx_{\text{ref1}}$, although it remains higher than in the original geometry, where the receiver was located at the center. Additionally, the MSE, RMSE, and MAE follow the same pattern as in previous measurements, with no significant differences for $W_n = 5$, 7, and 11.

Although the errors at both reference points appear slightly amplified, the goal of this work is to analyze the limitations of LoRa BastWAN boards. Furthermore, the achieved accuracy is sufficient to determine whether the transmitter is located within the laboratory space.

### 3.6.1 WLS via Gauss–Newton

In this part, we aim to compare the position estimates with those from a well known approach, the WLS method, implemented using the Gauss–Newton (GN) algorithm. The GN method is widely used to solve the nonlinear least squares problem found in position estimation from range measurements to known anchors. Estimating positions in trilateration scenarios often relies on recursive, non-linear optimization techniques, such as the Newton method or gradient based schemes [49]. Several alternative solutions have been proposed, for example in [50]. However, for fast benchmarking, we focus on the results obtained using the GN method.

For the configuration of GN algorithm, two covariance matrices $\mathbf{Q}$ were established, one based on the literature defined as $\mathbf{Q}_1 = [1\,0\,0; 0\,1\,0; 0\,0\,1]$, and $\mathbf{Q}_2$ based on the variances of the distance estimates derived from RSSI measurements. Assuming that the shadowing effects are independent and identically distributed, $\mathbf{Q}$ is a diagonal matrix that can be defined as [51]:

$$\mathbf{Q} = \text{diag}\left(\frac{1}{\sigma_1^2}, \frac{1}{\sigma_2^2}, \ldots, \frac{1}{\sigma_i^2}\right) \tag{21}$$

where $\sigma_i$ is the variance of distance measurements.

For the GN algorithm, the initial position was set at two different points to analyze the impact of initialization on convergence, one, $\text{In}_1$, near the center of the Power Electronics Laboratory at (4, 4), and a second, $\text{In}_2$, at (0, 0). The number of iterations was fixed at 1000, increasing this value did not improve the results.

In a first test, without filtering the RSSI data and using the first reference position $Tx_{\text{ref1}}$ with $\mathbf{Q}_2$ and $\text{In}_1$, the GN algorithm estimated the transmitter location at (3.037, 3.092) m, yielding an MSE of 1.021 m. When using $\mathbf{Q}_1$ and $\text{In}_2$, the estimated position was (3.187, 2.893) m, with a lower MSE of 0.7878 m. Next, applying a MF with $W_n = 11$, along with $\mathbf{Q}_1$ and $\text{In}_2$, the GN estimated the position at (3.115, 2.867), resulting in an MSE of 0.8396 m. Using the same parameters with a MAF, the estimated position was again (3.187, 2.893), with an MSE of 0.7877 m.

For the second reference position $Tx_{\text{ref2}}$, using $\mathbf{Q}_2$ and $\text{In}_2$, the estimated coordinates were (3.724, 7.761), with an MSE of 1.2695 m. When using $\text{In}_2$ with $\mathbf{Q}_1$, the GN computed the position as (3.003, 7.982), with an MSE of 1.7170 m. Applying $W_n = 11$ with $\mathbf{Q}_1$ and $\text{In}_2$, the MF and MAF filters yielded MSE values of 1.1044 m and 0.9223 m, respectively.

The approximation based on an initial position different from (4, 4), combined with the estimated matrix $\mathbf{Q}_2$, resulted in an MSE exceeding 6 m. The best performance for the GN method was achieved by initializing at (0, 0) and using the $\mathbf{Q}_1$ matrix. Therefore, further research is needed to determine an optimal covariance matrix $\mathbf{Q}$, particularly through more detailed analysis of the RSSI measurements and the corresponding distance estimations.

The results from geometry modification experiments demonstrate that anchor placement significantly influences the resulting position uncertainty. Simulations involving variations in inter-receiver distances further highlight the importance of spatial diversity in minimizing localization error. The weighted least squares method, implemented via the Gauss–Newton algorithm, converges reliably when the initial estimate is close to the true location. However, empirical estimation of the covariance matrix $\mathbf{Q}$ from RSSI samples produces less accurate results compared to the use of an identity matrix, thereby reducing the overall robustness of the position estimation process.

## 4. Conclusions

This study introduced a novel strategy for indoor localization using LoRa technology, with the primary contribution being the effective optimization of the path loss exponent in conjunction with OLS-based trilateration and median filtering techniques. The experimental results confirmed that carefully tuning the path loss exponent, along with the application of a median filter with an optimal window size $W_n = 7$, can dramatically improve the accuracy of localization in diverse indoor settings. The proposed method, by using commercial LoRa devices, not only reduces the mean square error of estimated positions but also demonstrates its viability as a robust and cost efficient solution for real world applications.

To further validate the proposed methodology, an alternative receiver geometry was implemented in the Power Electronics Laboratory with two distinct reference transmitter positions. Despite observing slightly higher error values, particularly for the first reference location, filtering results using MF and MAF remained consistent for window sizes $W_n = 5$, $W_n = 7$, and $W_n = 11$, demonstrating the robustness of the smoothing process. The increased error observed in this experiment indicates that the spatial configuration significantly impacts measurement accuracy. Nevertheless, the achieved precision remains sufficient to determine whether the transmitter is located within the laboratory boundaries. Additionally, benchmark comparisons using the

Gauss–Newton algorithm for weighted least squares estimation revealed that proper initialization and covariance matrix selection are critical for minimizing positioning error. These findings highlight the practical limitations and prospects of LoRa based localization systems and point to the need for continued refinement of both algorithmic parameters and environmental modeling in future research.

Future work will investigate the impact of key LoRa parameters, such as spreading factor and bandwidth, on localization performance to strike the optimal balance between accuracy, communication reliability, and energy efficiency in diverse indoor environments. We will also integrate adaptive filtering and machine learning techniques to improve system adaptability across varying conditions and to support more dynamic scenarios. In parallel, we plan to refine the weighted least squares estimator by developing more accurate covariance models. To broaden application fields, we will implement real-time geofencing and event triggered alerts, enabling use cases such as asset tracking in smart warehouses, personnel monitoring in healthcare facilities, and automated navigation for indoor service robots. We will also incorporate sensor fusion, combining RSSI with inertial measurements or UWB ranging, and integrate cloud analytics platforms to support predictive maintenance and energy optimization in smart buildings across industrial, commercial, and residential environments.

# References


[1] ZAFARI, F., GKELIAS, A., LEUNG, K. K. A survey of indoor localization systems and technologies. *IEEE Communications Surveys & Tutorials*, 2019, vol. 21, no. 3, p. 2568–2599. DOI: 10.1109/COMST.2019.2911558

[2] KIM, K., LI, S., HEYDARIAAN, M., et al. Feasibility of LoRa for smart home indoor localization. *Applied Sciences*, 2021, vol. 11, no. 1, p. 1–20. DOI: 10.3390/app11010415

[3] PELANT, J., TLAMSA, Z., BENES, V., et al. BLE device indoor localization based on RSS fingerprinting mapped by propagation modes. In *Proceedings of the 27th International Conference Radioelektronika (RADIOELEKTRONIKA)*. Brno (Czech Republic). 2017, p. 1–5. DOI: 10.1109/RADIOELEK.2017.7937584

[4] ROZUM, S., KUFA, J., POLAK, L. Bluetooth low power portable indoor positioning system using SIMO approach. In *Proceedings of the 42nd International Conference on Telecommunications and Signal Processing (TSP)*. Budapest (Hungary). 2019, p. 228–231. DOI: 10.1109/TSP.2019.8769114

[5] SIMKA, M., POLAK, L. On the RSSI-based indoor localization employing LoRa in the 2.4 GHz ISM band. *Radioengineering*, 2022, vol. 31, no. 1, p. 135–143. DOI: 10.13164/re.2022.0135

[6] RAPPAPORT, T. S. *Wireless Communications Principles and Practice*. 2nd ed. Upper Saddle River (USA): Prentice Hall, 2002. ISBN: 0130422320

[7] TSE, D., VISWANATH, P. *Fundamentals of Wireless Communications*. 1st ed., rev. New Jersey (USA): Cambridge University Press, 2005. ISBN: 9780521845274

[8] VISWANATHAN, M. *Wireless Communication Systems in Matlab*. 2nd ed., rev. Singapore (Singapore): Independently published, 2020. ISBN: 9798648523210

[9] STRZODA, A., MARJASZ, R., GROCHLA, K. How accurate is LoRa positioning in realistic conditions? In *Proceedings of the 12th ACM International Symposium on Design and Analysis of Intelligent Vehicular Networks and Applications*. Montreal Quebec (Canada). 2022, p. 31–35. DOI: 10.1145/3551662.3561260

[10] CHEN, H., XING, F., YANG, Q., et al. A lightweight mobile-anchor-based multi-target outdoor localization scheme using LoRa communication. *IEEE Transactions on Green Communications and Networking*, 2023, vol. 7, no. 4, p. 1607–1619. DOI: 10.1109/TGCN.2023.3236630

[11] AZEVEDO, J. A., MENDOÇA, F. A critical review of the propagation models employed in LoRa systems. *Sensors*, 2024, vol. 24, no. 12, p. 1–41. DOI: 10.3390/s24123877

[12] ISA, A. A. H., IQBAL, M. T. Remote low-cost web-based battery monitoring system and control using LoRa communication technology. *Journal of Electronics and Electrical Engineering*, 2024, vol. 3, no. 1, p. 134–159. DOI: 10.37256/jeee.3120244173

[13] KRISHNA, G., SINGH, R., GEHLOT, A., et al. IoT-based real-time analysis of battery management system with long range communication and FLoRa. *Results in Engineering*, 2024, vol. 23, p. 1–11. DOI: 10.1016/j.rineng.2024.102770

[14] AHMED, M. A., GALLARDO, J. L., ZUNIGA, M. D., et al. LoRa based IoT platform for remote monitoring of large-scale agriculture farms in Chile. *Sensors*, 2022, vol. 22, no. 8, p. 1–22. DOI: 10.3390/s22082824

[15] GKOTSIOPOULOS, P., ZORBAS, D., DOULIGERIS, C. Performance determinants in LoRa networks: A literature review. *IEEE Communications Surveys & Tutorials*, 2021, vol. 23, no. 3, p. 1721–1758. DOI: 10.1109/COMST.2021.3090409

[16] SUN, Z., YANG, H., LIU, K., et al. Recent advances in LoRa: A comprehensive survey. *ACM Transactions on Sensor Networks*, 2022, vol. 18, no. 4, p. 1–44. DOI: 10.1145/3543856

[17] DE ALMEIDA, I. B. F., CHAFII, M., NIMR, A., et al. Alternative chirp spread spectrum techniques for LPWANs. *IEEE Transactions on Green Communications and Networking*, 2021, vol. 5, no. 4, p. 1846–1855. DOI: 10.1109/TGCN.2021.3085477

[18] AZIM, A. W., BAZZI, A., SHUBAIR, R., et al. Dual-mode chirp spread spectrum modulation. *IEEE Wireless Communications Letters*, 2022, vol. 11, no. 9, p. 1995–1999. DOI: 10.1109/LWC.2022.3190564

[19] MERHEJ, D., AHRIZ, I., ZERIOUL, L., et al. Joint RSS and ranging fingerprint for LoRa indoor localization. In *Proceedings of the IEEE Wireless Communications and Networking Conference (WCNC)*. Dubai (United Arab Emirates). 2024, p. 1–6. DOI: 10.1109/WCNC57260.2024.10570742

[20] MARQUEZ, L. E., CALLE, M. Understanding LoRa-based localization: Foundations and challenges. *IEEE Internet of Things Journal*, 2023, vol. 10, no. 13, p. 11185–11198. DOI: 10.1109/JIOT.2023.3248860

[21] NEHME, J. A., NICOLAS, C., HABIB, G., et al. Experimental study of LoRa performance: a concrete building case. In *Proceedings of the IEEE International Conference on Automation/XXIV Congress of the Chilean Association of Automatic Control (ICA-ACCA)*. Valparaíso (Chile). 2021, p. 1–6. DOI: 10.1109/ICAACCA51523.2021.9465230

[22] ZHONG, C., NIE, X. Feasibility of LoRa for smart home: real time and coverage considerations. *IEEE Internet of Things Journal*, 2024, vol. 11, no. 14, p. 25213–25226. DOI: 10.1109/JIOT.2024.3391761

[23] ROBLES-ENCISO, R., MORALES-ARAGÓN, I. P., SERNA-SABATER, A., et al. Lora, Zigbee and 5G propagation and transmission performance in an indoor environment at 868 MHz. *Sensors*, 2023, vol. 23, no. 6, p. 1–22. DOI: 10.3390/s23063283

[24] CHEN, H., YANG, J., HAO, Z., et al. Research on indoor positioning method based on LoRa-improved fingerprint localization algorithm. *Scientific Reports*, 2023, vol. 13, no. 1, p. 1–13. DOI: 10.1038/s41598-023-41250-x

[25] BIANCO, G. M., GIULIANO, R., MAZZENGA, F., et al. Multi-slope path loss and position estimation with grid search and experimental results. *IEEE Transactions on Signal and Information Processing over Networks*, 2021, vol. 7, p. 551–561. DOI: 10.1109/TSIPN.2021.3106693

[26] BERTOLDO, S., PAREDES, M., CAROSSO, L., et al. Empirical indoor propagation models for LoRa radio link in an office environment. In *Proceedings of the 13th European Conference on Antennas and Propagation (EuCAP)*. Krakow (Poland). 2019, p. 1–5. ISBN: 9788890701887

[27] VO, H., NGUYEN, V. H. L., TRAN, V. L., et al. Advanced path loss model for distance estimation using LoRaWAN network's received signal strength indicator (RSSI). *IEEE Access*, 2024, vol. 12, p. 83205–83216. DOI: 10.1109/ACCESS.2024.3412849

[28] CHEN, H., YANG, J., HAO, Z., et al. Research on indoor multi-floor positioning method based on LoRa. *Computer Networks*, 2024, vol. 254, p. 1–13. DOI: 10.1016/j.comnet.2024.110838

[29] KHAN, F. U., MIAN, A. N., MUSHTAQ, M. T. Experimental testbed evaluation of cell level indoor localization algorithm using Wi-Fi and LoRa protocols. *Ad Hoc Networks*, 2022, vol. 125, p. 1–13. DOI: 10.1016/j.adhoc.2021.102732

[30] HU, K., GU, C., CHEN, J. LTrack: a LoRa-based indoor tracking system for mobile robots. *IEEE Transactions on Vehicular Technology*, 2022, vol. 71, no. 4, p. 4264–4276. DOI: 10.1109/TVT.2022.3143526

[31] AL-EIDANI, O. H., AL-NAKKASH, A. H., HUSSEIN, O. A. Evaluation fingerprint localization outdoor KNN SVM ANN using LoRa. In *Proceedings of the AIP Conference Proceedings*. Al-Samawa (Iraq). 2024, vol. 3051, no. 1, p. 1–15. DOI: 10.1063/5.0191553

[32] PUROHIT, J., WANG, X., MAO, S., et al. Fingerprinting-based indoor and outdoor localization with LoRa and deep learning. In *Proceedings of the GLOBECOM 2020 IEEE Global Communications Conference*. Taipei (Taiwan). 2020, p. 1–6. DOI: 10.1109/GLOBECOM42002.2020.9322261

[33] OUAMEUR, M. A., CAZA-SZOKA, M., MASSICOTTE, D. Machine learning enabled tools and methods for indoor localization using low power wireless network. *Internet of Things*, 2020, vol. 12, p. 1–13. DOI: 10.1016/j.iot.2020.100300

[34] ZELENY, O., FRYZA, T., BRAVENEC, T., et al. Detection of room occupancy in smart buildings. *Radioengineering*, 2024, vol. 33, no. 3, p. 432–441. DOI: 10.13164/re.2024.0432

[35] SAIFULLIN, K., AL-SHATRI, H., ALOUINI, M. Communications over unlicensed sub-8 GHz spectrum: Opportunities and challenges. *arXiv*, 2024, p. 1–52. DOI: 10.48550/arXiv.2412.11002

[36] ITU RADIO REGULATIONS. *Radio Regulations (Articles)*. 468 p. [Online] Cited 2025-05-28. Available at: https://www.itu.int/hub/publication/r-reg-rr-2024/

[37] DERÉVIANCKINE, G. H. *Feasibility and Performance of a LoRa 2.4 GHz Network*. Doctoral thesis, INSA Lyon (France), 2024, 191 p. Available at: https://hal.science/tel-04858023

[38] WU, D., LIEBEHERR, J. A low-cost low-power LoRa mesh network for large-scale environmental sensing. *IEEE Internet of Things Journal*, 2023, vol. 10, no. 19, p. 16700–16714. DOI: 10.1109/JIOT.2023.3270237

[39] AG ELECTRONICA, MEXICO. *BAST-WAN: Tarjeta de Desarrollo LoRa Nucleo RAK4260 32 Bit (datasheet)*. 3 p. [Online] Cited 2025-05-28. Available at: https://agelectronica.lat/pdfs/textos/B/BAST-WAN.PDF

[40] LORA ALLIANCE, USA. *LoRaWAN® Specification v1.1 (datasheet)*. 101 p. [Online] Cited 2025-05-28. Available at: https://resources.lora-alliance.org/technical-specifications/lorawan-specification-v1-1

[41] MICROCHIP, USA. *SAM L21 Family (datasheet)*. 1158 p. [Online] Cited 2025-05-28. Available at: https://ww1.microchip.com/downloads/en/DeviceDoc/SAM_L21_Family_DataSheet_DS60001477C.pdf

[42] NAVIDI, W., MURPHY, W. S., HEREMAN, W. Statistical methods in surveying by trilateration. *Computational Statistics & Data Analysis*, 1998, vol. 27, no. 2, p. 209–227. DOI: 10.1016/S0167-9473(97)00053-4

[43] LAURILA, S. H. *Electronic Surveying in Practice*. 1st ed. New York (USA): John Wiley & Sons, 1983. ISBN: 9780471090212

[44] SPILKER, J. J., AXELRAD, P., PARKINSON, B. W., et al. *Global Positioning System: Theory and Applications*. 1st ed. Washington, DC (USA): American Institute of Aeronautics and Astronautics, 1996. ISBN: 9781563471063

[45] SEKHAR, C. R., DUTT, V. B. S. S. I., RAO, G. S. GDoP estimation using simulated annealing for GPS and IRNSS combined constellation. *Engineering Science and Technology, an International Journal*, 2016, vol. 19, no. 4, p. 1881–1886. DOI: 10.1016/j.jestch.2016.09.017

[46] MOLISCH, A. F., TUFVESSON, F., KAREDAL, J., et al. A survey on vehicle-to-vehicle propagation channels. *IEEE Wireless Communications*, 2009, vol. 16, no. 6, p. 12–22. DOI: 10.1109/MWC.2009.5361174

[47] PRATT, W. K. *Digital Image Processing: PIKS Scientific Inside*. 4th ed. Hoboken, New Jersey (USA): Wiley-Interscience, 2007. ISBN: 9780471767770

[48] BLACKLEDGE, J. M. *Digital Signal Processing: Mathematical and Computational Methods, Software Development and Applications*. Amsterdam (Netherlands): Elsevier, 2006. ISBN: 1904275265

[49] KAY, S. M. *Fundamentals of Statistical Signal Processing: Estimation Theory*. 1st ed. Upper Saddle River, NJ (USA): Prentice-Hall, 1993. ISBN: 9780133457117

[50] SANTOS, R., MATOS-CARVALHO, J. P.,TOMIC, S., et al. WLS algorithm for UAV navigation in satellite-less environments. *IET Wireless Sensor Systems*, 2022, vol. 12, no. 3–4, p. 93–102. DOI: 10.1049/wss2.12041

[51] WU, S., XU, D., LIU, S. Weighted linear least square localization algorithms for received signal strength. *Wireless Personal Communications*, 2013, vol. 72, p. 747–757. DOI: 10.1007/s11277-013-1040-0

# About the Authors . . .

**Reynel OLIVERA** was born in Oaxaca, México in 1977. He received the Bachelor degree in 2000 in Electromechanical Engineering from the Technological Institute of Isthmus (ITI), México and the M.Sc. degree in Electrical Engineering in 2003 from Guanajuato University. At present, he is a full-time Professor in the Autonomous University of Zacatecas in the Electronics Department, México. His research interests are digital signal processing, telecommunications, and power electronics.

**Jorge FLORES** received his B.S. in Engineering Communications and Electronics from the Autonomous University of Zacatecas in 1992. After, in 2000 and 2010 he received his M.Sc. and D.Sc. in Electronic & Telecommunications from CICESE, respectively. Afterwards, he has joined the electrical engineering faculty at Autonomous University of Zacatecas. His principal interests are satellite communications, wireless communications, resource allocation, and embedded digital communications design. At present, he coordinates the Zacatecas Regional Space Development Centre of the Mexican Space Agency.

**Roberto OLIVERA** was born in Oaxaca, México in 1977. He received the Bachelor's degree in 2000 in Electromechanical Engineering from the Technological Institute of Isthmus (ITI), México and the M.Sc. degree in Electrical Engineering in 2003 from Guanajuato University. At present, he is a full-time Professor in the Autonomous University of Zacatecas in the Electronics Department, México. His research interests are digital signal processing, embedded systems, and electronic instrumentation.

**Janette PEREZ** was born in Mexico in 1985. She received her B.S. degree in Communications and Electronics Engineering from the Universidad de Guanajuato in 2008, followed by an M.S. degree in Electrical Engineering with a specialization in Optoelectronics from the same university in 2013. She was a full-time Associate Professor at the Universidad Tecnológica de Salamanca in the field of mechatronics for six years. Her research interests include optomechatronics, automation systems, and fiber optics. Additionally, she has published several works in national and international high-impact congresses and journals. Currently, she is a Ph.D. student at the Universidad Autónoma de Zacatecas.

**Jorge MUNOZ** was born in Zacatecas, Mexico, in 1987. He received the B.S. degree in Communications and Electronics Engineering from the Universidad Autonoma de Zacatecas, in 2010, and the M.S. and Ph.D. degrees in Electrical Engineering from DICIS, Universidad de Guanajuato, in 2012 and 2018, respectively. He is currently a full-time Professor in the Autonomous University of Zacatecas in the Electronics Department, México. His research interests include digital signal and image processing, optimal filtering, and probability and statistics.